Analytical model of dislocation nucleation on a near-surface void under tensile surface stress

Aarne S. Pohjonen [a] , Flyura Djurabekova [a] , Antti Kuronen [a] ,
Steven P. Fitzgerald [b] & Kai Nordlund [a]

[a] Helsinki Institute of Physics and the Department of Physics,
Accelerator Laboratory, University of Helsinki, P. O. Box 43,
FIN-00014, Finland

[b] EURATOM/CCFE Fusion Association, Culham Science Centre,
Abingdon OX14 3DB, United Kingdom

First

Taylor & Francis
Taylor & Francis Group

Analytical model of dislocation nucleation on a near-surface void under tensile surface stress

Aarne S. Pohjonen[a]*, Flyura Djurabekova[a], Antti Kuronen[a],
Steven P. Fitzgerald[b] and Kai Nordlund[a]

[a]*Helsinki Institute of Physics and the Department of Physics, Accelerator Laboratory,
University of Helsinki, P. O. Box 43, FIN-00014, Finland;* [b]*EURATOM/CCFE Fusion
Association, Culham Science Centre, Abingdon OX14 3DB, United Kingdom*

We have analyzed in detail the mechanism leading to tip growth on a surface which operates via nucleation of dislocations on a near-surface void under tensile surface stress. We derived a simplified analytical model describing the relevant physical factors related to the observed linearity between the void radius and the maximum depth of the void for the growth to occur. The model is based on the direct numerical calculation of atomic level stresses in the simulated system. Based on the present model we can estimate this maximum depth for a void of a certain size under a given stress in the size range which is beyond the feasibility of the molecular dynamics simulation method.

Keywords: void; surface protrusion; dislocations; metal; surface; electrical breakdown; copper

1. Introduction

Understanding the initiation mechanisms of vacuum electrical breakdown under high electric fields is of great scientific and technological interest. For example, the development of the next generation of linear colliders is impeded by the frequent occurrence of electrical breakdowns near the metal surfaces of accelerating structures [1,2]. Damage due to electrical breakdowns is also relevant in the context of the future fusion test reactor, ITER, where the erosion of material due to electrical arcs on tungsten divertors [3] has been found to be comparable to the erosion due to sputtering [4].

Prior to breakdown, electron currents are measured originating from random spots on the cathode [5]. These currents can be explained by the local enhancement of the electric field due to the formation of protrusions on the cathode surface [5,6].

In this study, we investigate the effect of the tensile stress applied on a metal surface under the electric field due to the interaction of the surface charge and the field. The magnitude of the tensile stresses at high electric fields ($> \sim 100\,\mathrm{MV/m}$) can be sufficient to stimulate dislocation activity near the surface. This can lead to

---

*Corresponding author. Email: aarne.pohjonen@iki.fi

significant topological modifications on the surface. In a previous study we showed that a near-surface void acting as a stress concentrator can cause repetitive nucleation of dislocations, leading to the formation of a protrusion on the surface [7].

Dislocation nucleation on voids has been studied in numerous publications [8], however not in the context of a near-surface void. For instance, it has been well established that a void can grow under external stress by emitting dislocation loops [9]. By considering the elastic equilibrium between emitted dislocation loops and the void and lattice resistance, it has been found that the void growth depends on both external stress and void size [9]. The relation between the threshold stress needed to form a dislocation loop on a void and the size of the void has been studied in [10]. Considering the interaction between a dislocation loop and the void (but neglecting the nucleation event) the authors found that the formation of the loop on a ~ 100 Å radius void requires a stress of $2\sigma_y$, where σ_y is the yield strength of the material. Such stress might be present in structural applications [10]. For copper the required stress would be 140 MPa. Based on a two-dimensional analytical model [11,12] it was also shown that the critical stress for dislocation emission decreases as the void size increases.

The molecular dynamics (MD) method has been employed widely to study the subject [13–16]. It has been found that the coalescence of voids is dependent on geometrical factors, namely the void radius and the distance between the voids [15,16]. A quasi-continuum method has been used to investigate nano-void growth in aluminum and deformation under shear by dislocation nucleation and dislocation interactions during stress loading and unloading stages. It was shown that during the unloading stage, most of the dislocation population and void volume is recovered, but some residual dislocation density remained [17,18]. Studies of void deformation via the emission of specific shear loops can be found in [11,19], although the suggested mechanism is still under debate, which illustrates the necessity of further studies [19–21].

Earlier [7] we investigated dislocation nucleation on a near-surface void under tensile stress exerted on the surface using MD simulation. The dislocations that move perpendicular to the surface are of particular interest, since they are the main cause for the growth of a protrusion on the surface above the void. In the simulations we found that there is a maximal depth of void location where the nucleation of such a dislocation is still possible and that this parameter, H_{max}, depends linearly on the void radius r for nano-sized voids. The geometry is illustrated in Figure 1.

Here we have performed additional simulations and analyzed the results in more detail. Moreover, we present a model that gives a physical explanation for the constants of linearity obtained from a least squares fit to the simulation data.

2. Simulations

The simulations were performed in a similar manner to those reported in [7] by using the PARCAS MD code [22]. We also used LAMMPS [23] to analyze the atomic-level stresses of the system in detail. We chose Cu for the modeling surface, applying the Sabochick–Lam interatomic potential [24], well tested with respect to melting point and point defect properties [25]. The potential has been used earlier in a study [26]
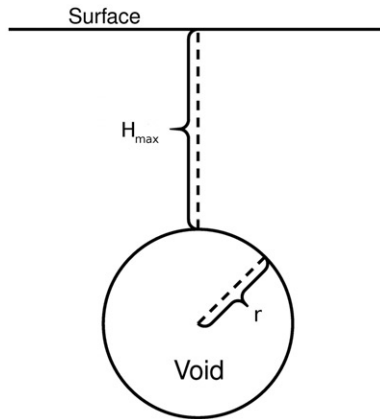
Figure 1. Illustration of the geometry of a near-surface void. The parameters relevant to the discussed mechanism are indicated. The maximum depth of the void, H_{max}, is defined in such a way that if the same void is placed below this depth, a dislocation never appeared during the MD simulation time.

involving surface properties (sintering) and dislocations. It was found that the surface energy calculated by the potential is in reasonable agreement with experimental values. We also found previously that the Mishin et al. [27] potential yielded qualitatively similar results to the Sabochick–Lam potential. In particular, the maximum depth H_{max} depended linearly on the radius of the void r in both cases, although the values of the constants of linearity were different. In the current simulations, a cell with a $\{110\}$ surface in the z-direction was constructed, with x- and y-axes in the $\langle 111 \rangle$ and $\langle 211 \rangle$ crystal directions, respectively. A schematic of the initial structure is shown in Figure 2. The size of the simulation cell was $22.4 \times 22.1 \times 16.8\,\text{nm}^3$ for voids of radius $r = 2.0, \ldots, 4.0\,\text{nm}$ under 4.58 GPa stress, $33.6 \times 33.5 \times 16.8\,\text{nm}^3$ for voids of radius $r = 3.5, \ldots, 5.0\,\text{nm}$ under 3.05 GPa stress and $33.6 \times 33.5 \times 21.9\,\text{nm}^3$ for voids of radius $r = 5.5\,\text{nm}$ under 3.05 GPa stress.

The tensile stress was applied on the surface in the following manner. In the beginning, the system was relaxed for 20 ps. After the relaxation, a linearly increasing force was applied to all atoms that initially formed the two top atomic layers until the maximum desired force was reached. Thus, initially in order to reach the equilibrium stress distribution and avoid the artificial rise of the stress waves, the stress was applied gradually with $\dot{\sigma} = 3.05$ GPa/100 ps. We have also paid particular attention to the fact that no dislocations were nucleated in the direction perpendicular to the surface during the stress ramping process. After that the system was held at the desired constant stress during the last 300 ps of the simulation time. The atoms located in the three atomic layers at the bottom of the simulation cell were not allowed to move, in order to prevent an undesired drift of the simulation box.

Since we were simulating the cells held under the different stresses, special attention was paid to the stress ramping process. If the desired stress is higher or lower, applying the same strain rate (to exclude the effect of the different strain rates on the dislocation nucleation process) in all cases will lead to an increase or decrease
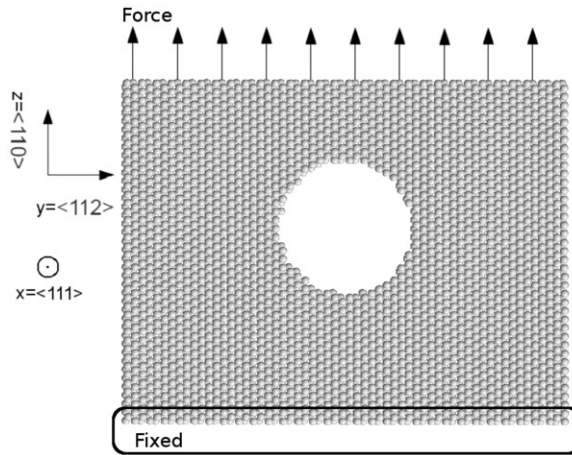
Figure 2. The simulation setup. A linearly increasing force was exerted on the top two layers of atoms. The atoms that formed the three bottom layers were held fixed during the simulation. The atoms within 7 Å of the lateral (*x*- and *y*-) boundaries were only allowed to move in the *z*-direction.

of the total simulation time, since the time for the constant stress simulations was fixed.

In order to examine the effect of time, we also performed simulations where the strain rate was not kept constant; on the contrary, it was allowed to change in order to keep fixed the duration of the ramping process and hence the entire simulation time (100 ps in all simulations, total time was 420 ps). Since the emission of dislocations perpendicular to surface direction was not observed during the ramping process in either sets of simulations, the different ramping scenarios did not affect the main conclusion of the maximum depth of the void. The observed differences were within the error bars.

To test how the simulation results could be extrapolated for larger voids or for lower surface stress, we conducted additional simulations. The simulation with 3.0 GPa surface stress with a void of radius $r = 9$ nm had cell dimensions $49.3 \times 44.3 \times 27.1$ nm^3. In order to increase the feasibility of the MD approach on this scale (a further lowering of the stress will inevitably lead to an increase of size dimensions), we changed the geometry of the simulation cell. Since we were interested in the maximal shear stress located on the upper hemisphere of the void, we bisected the simulation cell at the middle of the void. Using as the simulation cell only the upper part of the cell, we were able to increase the size of the void considerably, while the absent lower part was imitated by the three layers of fixed atoms around the void's cross-section. This also prevented cell drift during simulations. The atoms terminating the void surface above the level of fixed atoms were left to move freely. Such a trick enabled the systematic study of the nucleation process at fairly low stresses as well. We checked carefully that the stress distribution in the cell including half of the void was similar to the stress distribution in the cell with the whole void, confirming the possibility of such replacement.

In the simulations with 1.6 GPa surface stress and voids with 13 nm and 15 nm radius, the size of the simulation cell was $66.2 \times 93.7 \times 20.2 \, nm^3$. In the simulation with 1.6 GPa surface stress and 11 nm radius void the simulation cell size was $66.2 \times 93.7 \times 10.8 \, nm^3$.

Also, in the current work we performed the simulations assuming a special variety of boundary conditions in addition to the periodic ones. The atoms on the side borders were fixed in the x- and y-directions, while they were allowed to move in the z-direction. In this fashion the diagonal stacking faults, which appear during the simulation, are pinned at the borders without reappearing in the cell as would happen with periodic boundary conditions: The reappearance of the stacking faults in the cell occurs since the dislocations that move away from the void in diagonal directions cross the boundaries multiple times before arriving at the surface or the bottom of the simulation cell, causing artificial deformation and additional stress in the system.

A void with radius r was systematically placed with an interval of 2 Å at different depths below the surface. When the void was near to the surface, dislocations moving perpendicular to the surface were observed to cause growth of a tip on the surface. When the depth was increased, at some point the nucleation of such dislocations was not observed during the simulation time. This depth was defined as the critical depth, H_{max}.

The stacking faults, which appear between the leading and trailing partial dislocation, are shown in the snapshot of the 5 Å slice of the simulation cell (Figure 3). The atoms belonging to the stacking faults and surfaces were identified by calculating the centrosymmetry parameter P for the atoms

$$P = \sum_{i=1}^{i=6} |R_i + R_{-i}|^2 \tag{1}$$

where R_i and R_{-i} are the vectors corresponding to the six pairs of opposite nearest neighbors in the fcc lattice [28,29]. The dislocations which move perpendicular to the surface are the main reason for the formation of a protrusion on the surface. Prior to the nucleation of these dislocations, dislocations along {111} planes, which are not perpendicular to the surface, are nucleated in the simulations with a higher surface stress. In the simulations with the lower surface stress (≤ 1.6 GPa) the nucleation of these dislocations was not observed.

Since the shear stress on the slip plane is the driving force for dislocation nucleation, we analyzed the stress acting on the {111} slip plane, which has the normal in the x-direction in the simulation setup. The zx-component of the stress tensor, σ_{zx}, at the atomic positions was calculated using LAMMPS [23]. To avoid the random thermal fluctuations, the value of the stress tensor component was averaged over 1 ps.

3. Analytical model

In order to analyze the simulation results quantitatively, we postulate that the dislocation is nucleated at the point of maximum shear during the simulation, when the shear stress near the void surface exceeds a certain threshold value. It is well known that the dislocation nucleation mechanism on a free surface occurs via a
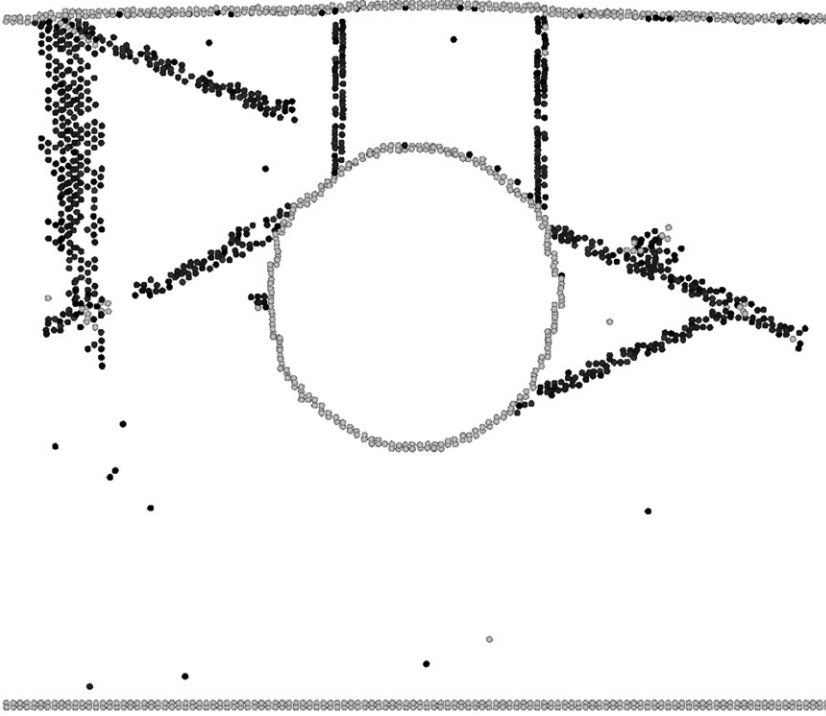
Figure 3. Stacking faults (black) created by dislocations which have nucleated on the void surface. The dislocations which move perpendicular to the surface are the main reason for the eventual formation of the protrusion on the surface. The atoms located on surfaces are colored gray. Only a 5 Å thick slice of the simulation frame is shown. The crystallographic orientations are the same as in Figure 2. The atoms belonging to the stacking faults and surfaces were identified by calculating the centrosymmetry parameter [28,29].

formation of a glide loop under shear stress. Once a glide loop (a dislocation line starting and ending on the void, and thus enclosing a certain area) bows out larger than a certain critical size, it will continue expanding [30–32]. We will hereafter refer to such a glide loop of critical size as a dislocation nucleus. Thus to expect the dislocation to be nucleated on the void surface it is necessary that the stress concentrated in the vicinity of the void is sufficient for the dislocation nucleus to be formed.

The geometry, which we shall use in the following description of the model, is illustrated in Figure 4a. In the description we employ the following definition of the stress vector: assume a closed surface S bounding a volume V. A vector surface element $\Delta A \vec{v}$ on the surface S with the unit surface normal $\vec{v}$ and area ΔA experiences a total force $\vec{F}$ by the exterior of S. The stress vector is defined as

$$\vec{T}^{\vec{v}} := \lim_{\Delta A \to 0} \frac{\vec{F}}{\Delta A}. \tag{2}$$
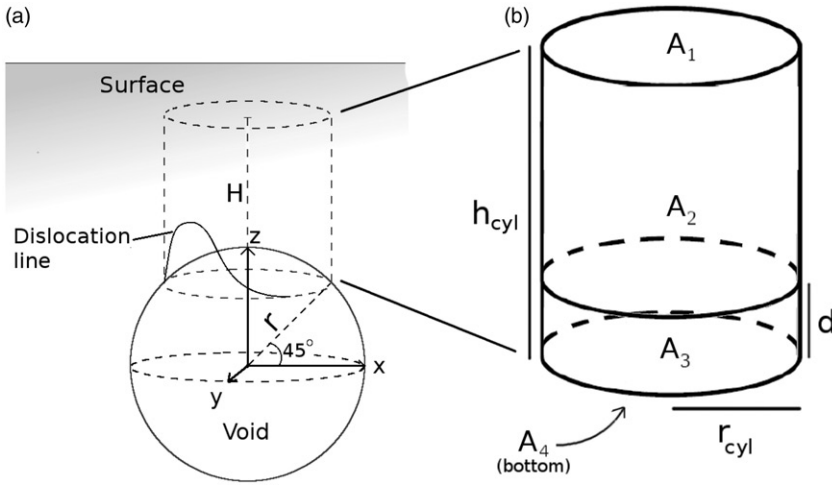
Figure 4. (a) The maximum shear stress is at the point where the shear direction is at a 45°
angle to the void surface [11]. (b) The description of the criterion for growth is obtained when
the surface integral of the stress vector over the glide cylinder of the dislocation is divided into
four subsurfaces.

Since the stress vector depends on the orientation of the surface element, it is denoted
by the superscript on the left-hand side of Equation (2) [33].

In equilibrium, the integral of the *z*-component of the stress vector over the entire
surface *S* circumscribing the cylindrical volume depicted in Figure 4 yields zero:

$$\int_S T_z^{\vec{v}} = 0. \tag{3}$$

Dividing the surface into four subsurfaces, as illustrated in Figure 4b, we obtain

$$\int_{A_1} T_z^{\vec{v}} + \int_{A_2} T_z^{\vec{v}} + \int_{A_3} T_z^{\vec{v}} + \int_{A_4} T_z^{\vec{v}} = 0 \tag{4}$$

where A_1 is the top of the cylinder located on the surface of the material, and A_2 and
A_3 are the walls of the two sub-cylinders having heights $h_{cyl} - d$ and d, where h_{cyl} is
the height of the original cylinder and d is the height of the lower sub-cylinder. The
latter can also be understood as the height of the dislocation nucleus. The rim of
the cylinder is contained in A_3. A_4 is the bottom of the cylindrical volume. The
integral over A_4 is zero since there is no force applied downwards in this region (the
ceiling of the void) by the exterior of *S*. The integrals can be replaced by the product
of the average of the function $T_z^{\vec{v}}$ over the surface area where this function is
integrated and the area itself, yielding

$$\pi r_{cyl}^2 \langle T_z^{\vec{v}} \rangle_{A_1} + 2\pi r_{cyl}(h_{cyl} - d)\langle T_z^{\vec{v}} \rangle_{A_2} + 2\pi r_{cyl} d \langle T_z^{\vec{v}} \rangle_{A_3} = 0 \tag{5}$$

where r_{cyl} is the radius of the cylinder. Regions where the stress is averaged are
indicated by the subscript. We define the threshold average stress B_3 as the minimum

average stress exerted on A_3 required for a dislocation to be nucleated at a given time and temperature. Assuming homogeneous external surface stress of magnitude T^{ext} directed in the z-direction, we can lighten the notation and denote $\langle T_z^{\vec{v}} \rangle_{A_1} = T^{\mathrm{ext}}$.

To compare the results derived from our model to the values obtained by others, we calculate an estimate for the activation volume Ω based on the parameter d of the model. Observations of the simulation results (see Figure 8) show that we can approximate the parameter d as the radius of the semicircular dislocation nucleus (cf. Figure 8): $\Omega = A_c |\vec{b}|$, where $\vec{b}$ is the Burgers vector of the nucleating partial dislocation and A_c is the area enclosed by the dislocation nucleus [34]. This yields

$$\Omega = \frac{\pi d^2}{2} |\vec{b}|. \tag{6}$$

The activation volume is a function of the local shear stress and temperature. Since the local shear stress is constant, B_3, in the model, the parameter d has no dependence on surface stress.

We saw in our simulations that the dislocation was nucleated almost immediately if the void was located very near to the surface. We did not observe the nucleation of dislocations at the deeper voids, at least during the simulation time span. Hence we conclude that there must exist a maximum depth, $h_{\mathrm{cyl}}^{\max}$, for the dislocation to be nucleated. Assume that the void is located at this maximal depth, $h_{\mathrm{cyl}} = h_{\mathrm{cyl}}^{\max}(r_{\mathrm{cyl}})$. At this depth, the stress needed to nucleate the dislocation $B_3 = \langle T_z^{\vec{v}} \rangle_{A_3}$ can be determined as a constant for a given material and temperature. It is possible that over longer times the dislocation could nucleate under lower stress, hence B_3 can depend on the simulation time. Now we solve Equation (4) with respect to the value of the stress applied to the region A_2, denoted B_2:

$$B_2 = \frac{-T^{\mathrm{ext}} r_{\mathrm{cyl}} - 2dB_3}{2(h_{\mathrm{cyl}}^{\max}(r_{\mathrm{cyl}}) - d)}. \tag{7}$$

This equation gives us the opportunity to define the depth where the concentration of the shear stress can still be sufficient to emit the dislocation. Thus in the steady state a dislocation will be emitted if

$$h_{\mathrm{cyl}} \leq h_{\mathrm{cyl}}^{\max}(r_{\mathrm{cyl}}) = \frac{-T^{\mathrm{ext}}}{2B_2} r_{\mathrm{cyl}} + \mathrm{d}\left(1 - \frac{B_3}{B_2}\right). \tag{8}$$

In general, this criterion is applicable to a wide range of times and temperatures. However, we note that the parameters B_2 and B_3 can be overestimated if the system evolution is analyzed during a short time as dictated by the limited MD time span (B_2 and B_3 are the shear stress averaged over the different areas). The exaggeration of the stress in the system allows us to observe the dislocation nucleation during the simulation time span because the local shear stress affects the activation barriers for the nucleation of dislocations (the nucleation event is thermally activated). The different simulation times and temperatures might introduce an uncertainty in the estimation of these parameters; this is why for consistency we performed all the simulations at a fixed time and temperature. Moreover, it is not clear whether these parameters exhibit the void-size dependence. We analyzed the critical average stresses B_2 and B_3 by calculating the atomic level stress on each atom for the voids

positioned $1\,\text{Å}$ below the maximum depth for dislocation nucleation. We found that in the range of radii of the voids investigated in the present study, both parameters B_2 and B_3 remained independent of r_{cyl} within the accuracy obtained in the simulations (cf. Figure 10).

Here we investigate the dependence of h_{cyl}^{max} instead of H_{max} on r as in [7], shown in Figures 1 and 4. The super/subscript 'max' again denotes the extreme case when the void is located at the depth where the growth of the tip still occurs within the simulation time at the given stress and temperature. The radius of the void r is related to r_{cyl} as

$$r_{cyl} = \frac{r}{\sqrt{2}} \tag{9}$$

and h_{cyl}^{max} is related to H_{max} as

$$h_{cyl}^{max} = H_{max} + \left(\sqrt{2} - 1\right)r_{cyl} \tag{10}$$

by geometry, as shown in Figure 4. The observed linearity in the variables h_{cyl}^{max} and r_{cyl} is equivalent to the linearity between the variables H_{max} and r:

$$h_{cyl}^{max} = ar_{cyl} + c \Leftrightarrow H_{max} = \left(\frac{a+1}{\sqrt{2}} - 1\right)r + c. \tag{11}$$

4. Results

Comparison of the results of our analytical model and the simulation results can give an insight into the mechanisms of the growth of a surface protrusion under static tensile stress. For this purpose we numerically analyzed the *zx*-component of the stress acting on the {111}-slip plane, calculated for each atom with MD. This result is shown in Figure 6.

The maximum shear stress is found approximately at the point where the void surface is at a 45° degree angle to the shear (dotted line, Figure 5), as suggested by Lubarda et al. [11]. We further analyzed the shear stress field along the vertical line which passes through the point of maximum shear. From Cauchy's postulate [35] it follows directly that the absolute values of the stress vector with surface normal in the *x*-direction and the *zx*-component of the stress tensor are equal: $|T_z^{\hat{x}}| = |\sigma_{zx}|$.

We have performed a set of systematic simulations using the technique described in Section 2. In Figure 6 we plot the maximum height of the cylinder versus the radius of the cylinder $h_{cyl}^{max}(r_{cyl})$ in accordance with the model described in Section 3 for two external stresses $4.58\,\text{GPa}$ and $3.05\,\text{GPa}$ applied at the surface (Figure 6). The error bars indicate the uncertainty of defining the maximum depth where the concentrated stress near the void reaches the critical value sufficient to create a dislocation nucleus. The simulation results can be linearly fit as follows:

$$h_{cyl}^{max}(r_{cyl}) = ar_{cyl} + c. \tag{12}$$
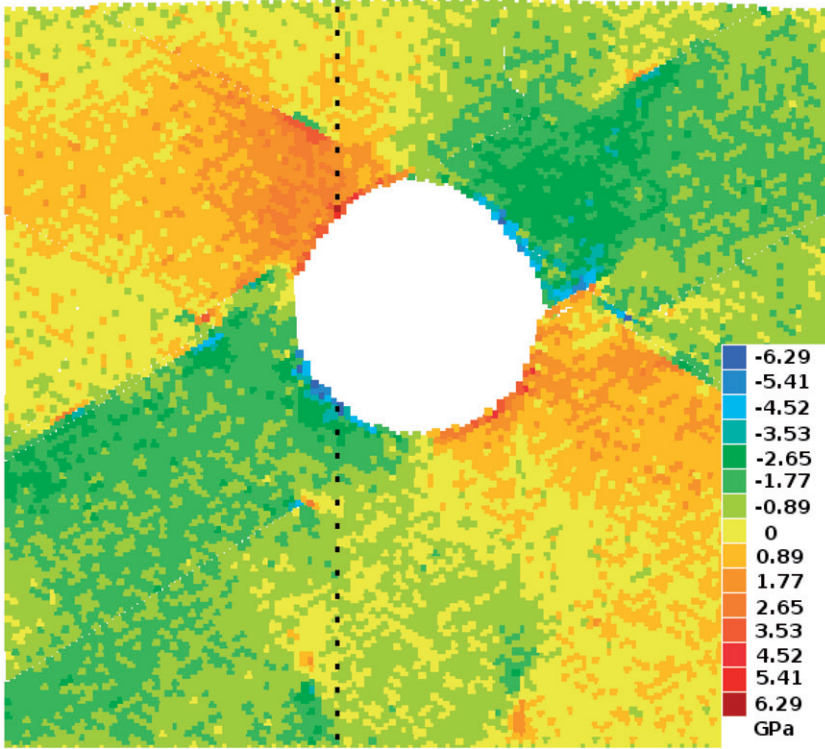
Figure 5. The shear stress field σ_{zx} perpendicular to the slip plane (the slip plane is in the direction of the *x*-axis) when the void is 1 Å below H_{max}. The void radius $r = 40$ Å. The vertical line where the shear stresses of atoms were further analyzed is marked with a dashed line. Dislocations that move in diagonal directions have been nucleated, but no dislocation moving perpendicular to the surface has nucleated on the analyzed {111} slip plane.
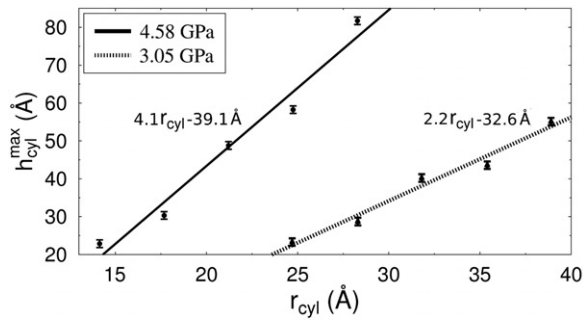
Figure 6. The least squares fit to the (r_{cyl}, h_{cyl}^{max}) data shows that the dependence is approximately linear for the simulated nano-scale voids. The corresponding void radii were $r = 20, \ldots, 40$ Å for 4.58 GPa surface stress and $r = 35, \ldots, 55$ Å for 3.05 GPa surface stress.

The coefficients of the fit a and c give a quantitative description of the dependence $h_{\mathrm{cyl}}^{\max}(\langle T_z^{\vec{v}} \rangle)$. Comparing (12) and (8) we find:

$$a = \frac{-T^{\mathrm{ext}}}{2B_2} \tag{13}$$

and

$$c = \mathrm{d}\left(1 - \frac{B_3}{B_2}\right). \tag{14}$$

The investigation of these coefficients can assist in understanding the void size effect on dislocation nucleation on a near-surface void under tensile stress.

The parameters a and c are obtained from the fit (12). However, there are three unknowns in Equations (13) and (14): d, B_2 and B_3. The values of B_2 and B_3 depend on the distance d, hence it is natural to take d as the free parameter which is to be determined based on the calculation of atomic level stress by the following procedure. We calculated the average shear stress B_3^{atomic} within the different heights d from the void surface as an average of the atom-level stress for voids of different radii. This value was compared to the value B_3^{fit} obtained from the least squares fitting of data in Figure 6 in terms of Equations (13) and (14). Testing the different values of d we minimized the difference $\Delta B_3 = B_3^{\mathrm{atomic}} - B_3^{\mathrm{fit}}$ as shown in Figure 7. It is clear that the best correspondence is found for the approximate value $d = 3|\vec{b}|$, where $|\vec{b}|$ is the Burgers vector of the nucleating partial dislocation with Burgers vector $\vec{b} = a/6\langle 112 \rangle$, where a is the lattice constant. Then, adopting the estimated value of d, Equation (6) gives the value of the activation volume $\Omega = 22|\vec{b}|^3$, which is comparable to the values obtained by other groups for dislocation nucleation on the surface (nano-pillars), $\Omega = (1-10)|\vec{b}|^3$ [30] and $\Omega = (2-30)|\vec{b}|^3$ [31]. The shear stress σ_{zx} along the axes drawn through the point of maximum shear stress (the vertical line in Figure 5) is shown in Figure 9. The points which were averaged to obtain the parameters B_3^{atomic} within the obtained value of d, and B_2^{atomic}, which is further than d from the void surface, are indicated separately.

The nucleation event of the leading partial dislocation on the void surface is shown in Figure 8. The inset demonstrates the dislocation nucleus with the height compared to the distance d.

Now, knowing the value $d = 3|\vec{b}|$ we can estimate the parameters B_2 and B_3 from Equations (13) and (14). In Table 1 we report these parameters for two different sets of simulations (the different surface stresses). The obtained value of $B_3 = 5.4\,\mathrm{GPa}$ is consistent for both cases and can be compared to the theoretical shear strength of copper $\sim \frac{\mu}{15} = 3.1\,\mathrm{GPa}$ [32,36] (μ is the shear modulus of copper) or the ideal simple shear strength, $\sim 3.4\,\mathrm{GPa}$ [37]. The analysis of the parameter B_2 is more obscure since the small difference in these values for both stresses might lie within the error bars determined for this quantity.

In order to investigate whether the parameters B_2 and B_3 depend on the size of the void, in Figure 10 we plot the averages of the σ_{zx} stress component on the atoms further away from the void (B_2^{atomic}) and right at the void surface within the distance d (B_3^{atomic}) versus the void radii. Visual inspection of the graph confirms that both parameters steadily fluctuate around the average values ($5.4 \pm 0.3\,\mathrm{GPa}$ for B_3^{atomic}
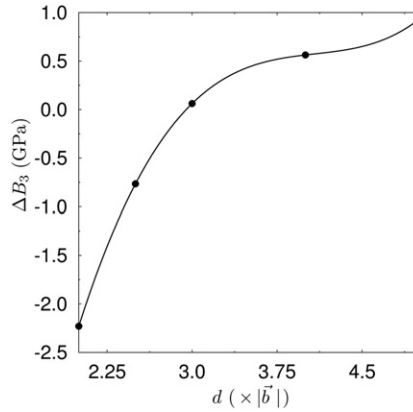
Figure 7. The difference $\Delta B_3(d)$ between B_3^{atomic} obtained by calculating the atomic level stress, and B_3^{fit} obtained from the least squares fit to the simulation results for different values of the distance d (dots). A fourth-order polynomial is fitted to the data (solid line). The difference reaches zero at approximately $d = 3|\vec{b}|$, where $\vec{b}$ is the Burgers vector of the nucleating partial dislocation.
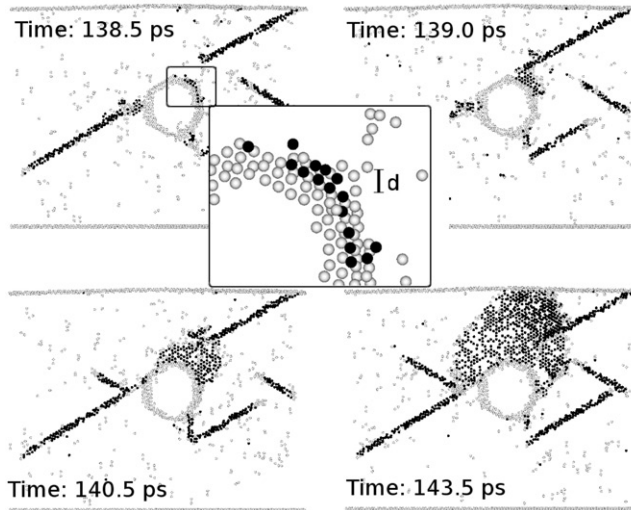
Figure 8. Nucleation of dislocation on the slip plane which is perpendicular to the surface. The mechanism proceeds when the dislocation loop grows larger than the critical size [30–32]. The distance d, which was obtained by comparing the analytical model to the atomic level stress, shows the critical size of the loop. Atoms belonging to a stacking fault, which is formed behind the leading partial dislocation, are colored in black and atoms belonging to a surface are colored in gray. Only a 5 Å thick slice of the simulation snapshot is shown.

and $1.3 \pm 0.1\,\text{GPa}$ for B_2^{atomic}). For comparison we also added the values taken from Table 1 (horizontal lines). As one can see the values of both parameters calculated in two different ways agree very well. The discrepancy between the values of B_2^{atomic} and B_2^{fit} can be explained by the simplifications of the analytical model underlying the
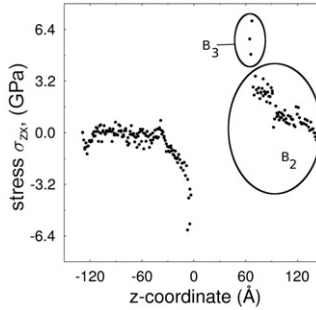
Figure 9. The shear stress of the atoms on the vertical line shown in Figure 5 through the point of maximum shear as a function of the z-coordinate of the atoms when the void is directly below H_{max}. The stress of the atoms used to calculate the average stresses B_2 and B_3 are indicated by the ellipses.

Table 1. The average stresses over areas A_1, A_2 and A_3, when the void is 1 Å below the maximal depth H_{max} for dislocation nucleation. B_2^{fit} and B_3^{fit} stand for the average stress over regions A_2 and A_3, respectively.

Surface stress, T^{ext} (GPa)	B_2^{fit} (GPa)	B_3^{fit} (GPa)
4.58	-0.56 ± 0.07	-5.4 ± 1.5
3.05	-0.69 ± 0.06	-5.4 ± 1.1

value B_2^{fit} obtained from the fitting to the simulation data. Thus the direct calculation of σ_{zx} shows that B_2 can indeed be approximated as a constant at the given stress, as assumed in the model.

The superposition of the nucleation rim radii r_{cyl} of the cylindrical volume used in the model and the shape of the protrusion (viewed from above) that was grown on the surface due to dislocations moving perpendicular to the surface gives good agreement (Figure 11). The shape of the protrusion is rhomboidal, which was discussed in [7] and can be explained by the face-centered-cubic crystal structure, which has two glissile {111} planes, perpendicular to the {110} surface and forming a 71° angle in-between. The difference in the shapes of a protrusion and the assumed cylinder can also affect the discrepancy for B_2 seen in Figure 10.

The suggested model aims to give a comprehensive view of the dislocation nucleation event on a near-surface void under tensile stress applied on the surface due to a high electric field and extract information useful for the prediction of the relevance of this mechanism on the experimental time scales. Since the simulated voids are of nano-size, it is of prime importance to understand the finite-size effect on this mechanism. With this purpose we studied the geometric properties of the proposed mechanism. Namely, we investigated the aspect ratio γ of the depth h_{cyl}^{max} of the point where the concentration of the shear stress on the void surface is maximal
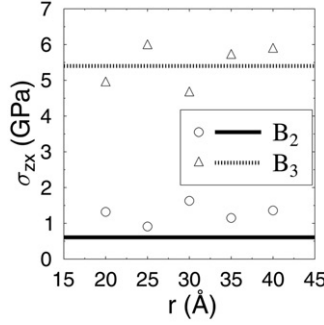
Figure 10. The average value of the σ_{zx} stress component within distance $d = 3|\vec{b}|$ from the void surface (triangles) corresponding to the value of B_3^{atomic} (dashed line for B_3^{fit}) and the average value of the stress component further away (circles) corresponding to B_2^{atomic} (solid line for B_2^{fit}) as a function of the void radius when the void depth is directly below $H_{\max}$. The surface stress magnitude was 4.58 GPa.

and sufficient to create a dislocation nucleus to the radius r of the void, $\gamma = h_{\text{cyl}}^{\max}/r$. Using Equation (9), Equation (8) can be rewritten as follows:

$$\gamma = \frac{h_{\text{cyl}}^{\max}}{r} = \frac{-T^{\text{ext}}}{2\sqrt{2}B_2} + \frac{\mathrm{d}\left(1 - \frac{B_3}{B_2}\right)}{r}. \tag{15}$$

The analysis of this dependence reveals that for large voids ($r \gg d(1 - \frac{B_3}{B_2})$) the second term describing the finite-size effect becomes insignificant and γ of the considered geometry will be defined only by the relation of the external stress to the shear stress created between the void and the surface. We plotted the simulation results interpreted in terms of Equation (15) for both investigated stresses 3.05 GPa and 4.58 GPa (Figure 12). As one can see in both cases we are in the regime when the finite-size effect is significant and the considered aspect ratio does not remain constant with the void radius. Using again the least squares fitting technique, we obtain the inverse function

$$\gamma = \frac{h_{\text{cyl}}^{\max}(r)}{r} = \frac{a}{\sqrt{2}} + \frac{c}{r},$$

where a and c are similar fitting coefficients as in Figure 6.

In order to test our model we made additional simulations with an external stress of about half of 3.05 GPa (1.6 GPa) for the larger voids ($r > 10$ nm). In this case we were forced to use the cell with the hemisphere as described in Section 2. The results are also present in the same graph in Figure 12. In this case it is clear that we overcame the region of the finite-size effect as all three points are clearly lying almost on the same line. The best fit to this data we obtained assuming the increase of the parameter B_2 is linear, and the coefficient of linear proportionality is estimated from the values of B_2 presented in Table 1. We explain this observation by the change of the geometry (the void size versus the depth of the maximum shear stress) for each
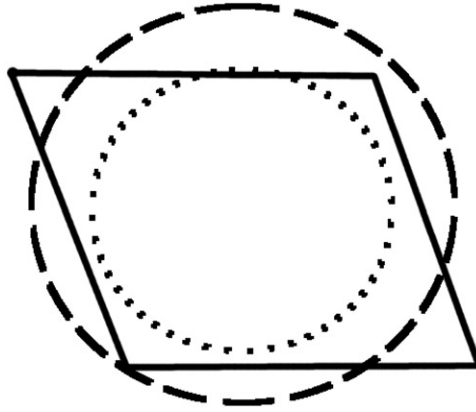
Figure 11. The shape of the tip grown on the surface viewed from above (solid line) is compared to the void shape (dashed line) and to the nucleation rim of radius r_{cyl} (dotted line) used in the analytical model.
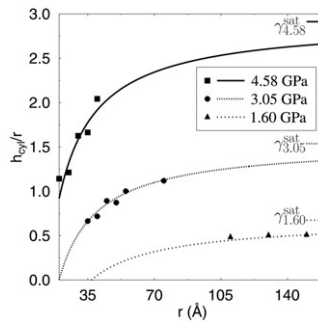
Figure 12. Aspect ratio γ of the depth of the maximal shear stress sufficient to create a dislocation nucleus and the radius of the void as a function of the void radius. The results are shown for two investigated external stresses 3.05 GPa and 4.58 GPa. The points obtained for the lower stress (1.6 GPa) are added for prediction purposes. The lines are the inverse functions (Equation 15), where a and c are calculated with the parameters B_2 and B_3 from Table 1. The low stress data was fit based on the same value B_3; B_2 was increased with the linear proportionality assumed for the increase in B_2 from the higher value (B_2 of external stress ($T = 4.58$ GPa) to the lower one $T = 3.05$ GPa) in Table 1 (see text). The horizontal lines on the right side of the figure indicate the corresponding level of $\gamma^{sat} = a$, where a is defined in Equation (13).

stress, which will definitely affect the distribution of the stresses between the void and the surface. More information from this graph can be derived on the saturated value of γ denoted as γ^{sat}, when the scale invariance of the stress distribution holds for a given external stress. This information can be used to estimate the potential risk of the formation of prismatic loops [7] on a void of macroscopic size, which is certainly beyond the range of the atomistic simulations. We emphasize that the model does

not depend directly on the absolute values of the parameters B_2 and B_3, which were defined in this work based on the atomistic simulations. Using instead the values estimated from the macroscopic considerations in the regime of γ^{sat}, the model can also be used on macroscopic time scales.

5. Conclusions

We have analyzed the effect of void size on the mechanism that can lead to the growth of a tip on a surface under an electric-field-induced stress. Such a stress can appear on the metal surface as a result of the effect of high electric fields (for instance, $E \sim 10\,\text{GV/m}$ corresponds to surface stress $T = 0.9\,\text{GPa}$). The mechanism operates via nucleation of dislocations on near-surface voids under static tensile stress exerted on the surface [7]. Here we propose an analytical model to explain the process of tip growth via this mechanism. Based on the model, we give a physical explanation of the coefficients of linearity in the criterion for growth observed earlier [7]. We observed that the dislocations are nucleated on the void during the simulation if the shear stress is concentrated sufficiently near the surface of the void to create a dislocation nucleus. The ratio of the critical depth, where such a nucleus is still created, to the radius of the void defines the geometric aspect ratio γ that gives a high probability of dislocation nucleation for a given stress. We also observed a clear finite-size effect, which decreases the value of γ, and must be taken into account when the size of the void is comparable to the size of the dislocation nucleus. In the macroscopic limit, γ reaches the value $\gamma^{\text{sat}} = T^{\text{ext}}/2\sqrt{2}\langle\sigma_{zx}\rangle$, where T^{ext} is the external tensile stress on the surface and $\langle\sigma_{zx}\rangle$ is the average shear stress distributed between the point of σ_{zx}^{max} on the surface of the void and the surface.

Acknowledgments

References

[1] W. Wuensch, AIP Conf. Proc. 877 (2006) p. 15.
[2] A. Descoeudres, T. Ramsvik, S. Calatroni, M. Taborelli and W. Wuensch, Phys. Rev. ST Accel. Beams 12 (2009) p.032001.
[3] N. Holtkamp, Fusion Eng. Design 84 (2009) p.98.
[4] V. Rohde, *Arc surface damage in fusion reactors*, in *Breakdown Physics Workshop*, CERN, 6–7 May 2010.

[5] R. Boxman, *Handbook of Vacuum Arc Science and Technology*, Noyes Publications, Bracknell, 1995.
[6] R.V. Latham, Phys. Technol. 9 (1978) p.20.
[7] A. Pohjonen, F. Djurabekova, A. Kuronen, K. Nordlund and S. Fitzgerald, J. Appl. Phys. 110 (2011) Article no. 023509.
[8] M. Meyers, S. Traiviratana, V. Lubarda, D. Benson and E. Bringa, J. Miner. Metals Mater. Soc. 61 (2009) p.35.
[9] D.C. Ahn, P. Sofronis and R. Minich, J. Mech. Phys. Solids 54 (2006) p.735.
[10] D.C. Ahn, P. Sofronis, M. Kumar, J. Belak and R. Minich, J. Appl. Phys. 101 (2007) Article no. 063514.
[11] V. Lubarda, M. Schneider, D. Kalantar, B. Remington and M. Meyers, Acta Mater. 52 (2004) p.1397.
[12] T.C. Tszeng, J. Appl. Phys. 103 (2008) Article no. 053509.
[13] E. Rudd and J. Belak, Comp. Mater. Sci. 24 (2002) p.148.
[14] R. Rudd, E. Seppala, L. Dupuy and J. Belak, J. Computer-Aided Mater. Design 14 (2007) p.425.
[15] E. Seppala, J. Belak and R. Rudd, Phys. Rev. Lett. 93 (2004) p.245503.
[16] E. Seppala, J. Belak and R. Rudd, Phys. Rev. B 71 (2005) p.064112.
[17] J. Marian, J. Knap and M. Ortiz, Phys. Rev. Lett. 93 (2004) Article no. 165503.
[18] J. Marian, J. Knap and M. Ortiz, Acta Mater. 53 (2005) p.2893.
[19] E. Bringa, S. Traiviratana and M. Meyers, Acta Mater. 58 (2010) p.4458.
[20] V.V. Bulatov, W.G. Wolfer and M. Kumar, Scripta Mater. 63 (2010) p.144.
[21] E.M. Bringa, V.A. Lubarda and M.A. Meyers, Scripta Mater. 63 (2010) p.148.
[22] K. Nordlund (2010), PARCAS computer code; private communication.
[23] S. Plimpton, J Comp. Phys. 117 (1995) p.1.
[24] M.J. Sabochick and N.Q. Lam, Phys. Rev. B 43 (1991) p.5243.
[25] K. Nordlund and R.S. Averback, Phys. Rev. Lett. 80 (1998) p.4201.
[26] H. Zhu, Phil. Mag. Lett. 73 (1996) p.27.
[27] Y. Mishin, M.J. Mehl, D.A. Papaconstantopoulos, A.F. Voter and J.D. Kress, Phys. Rev. B 63 (2001) p.224106.
[28] J. Knap and M. Ortiz, Phys. Rev. Lett. 90 (2003) p.226102.
[29] C. Kelchner, S. Plimpton and J. Hamilton, Phys. Rev. B 58 (1998) p.11085.
[30] T. Zhu, J. Li, A. Samanta, A. Leach and K. Gall, Phys. Rev. Lett. 100 (2008) p.025502.
[31] J. Li, MRS Bull. 32 (2007) p.151.
[32] J.P Hirth and J. Lothe, *Theory of Dislocations*, 2nd ed., Krieger, Malabar, Florida, 1992.
[33] I. Sokolnikoff, *Mathematical Theory of Elasticity*, McGraw-Hill, New York, 1956.
[34] S. Ryu, K. Kang and W. Cai, J. Mater. Res. 26 (2011) p.2335.
[35] D.R. Smith, *An Introduction to Continuum Mechanics*, Kluwer Academic, Dordrecht, 1993.
[36] W.D. Callister Jr, *Materials Science and Engineering. An Introduction*, 3rd ed., John Wiley, New York, 1993.
[37] S. Ogata, J. Li and S. Yip, Science 298 (2002) p.807.